UNCLASSIFIED
SECURITY CLASSIFICATION

AD-A273 466

(2)

N PAGE

1a. REPORT SECURITY CLA — CTIVE MARKINGS

2a. SECURITY CLASSIFICATION AUTHORITY

2b. DECLASSIFICATION/DOWNGRADING SCHEDULE

DEC 07 1993

3. DISTRIBUTION/AVAILABILITY OF REPORT
APPROVED FOR PUBLIC RELEASE:
DISTRIBUTION UNLIMITED

4. PERFORMING ORGANIZATION RT NUMBER(S)

5. MONITORING ORGANIZATION REPORT NUMBER(S)
AFOSR-TR- 93 0870

6a. NAME OF PERFORMING ORGANIZATION	6b. OFFICE SYMBOL (If applicable)	7a. NAME OF MONITORING ORGANIZATION
Princeton University		Dir. of Chemistry and Materials Science AFOSR/NC

6c. ADDRESS (City, State, and ZIP Code)	7b. ADDRESS (City, State and ZIP Code)
A313 Hayes Hall, Engineering Quadrangle Princeton, NJ 08544-5263	110 Duncan Avenue, Suite B115 Bolling AFB, DC 20332-0001

8a. NAME OF FUNDING/SPONSORING ORGANIZATION	8b. OFFICE SYMBOL (If applicable)	9. PROCUREMENT INSTRUMENT IDENTIFICATION NUMBER
AFOSR	NC	AFOSR-91-0040

8c. ADDRESS (City, State, and ZIP Code)	10. SOURCE OF FUNDING NOS.			
	PROGRAM ELEMENT NO.	PROJECT NO.	TASK NO.	WORK UNIT NO.
110 Duncan Avenue, Suite B115 Bolling AFB, DC 20332-0001	61102F	2303	BS	

11. TITLE (Include Security Classification)
Nanodesigning of Hierarchical Multifunctional Ceramics

12. PERSONAL AUTHOR(S)
Ilhan A. Aksay, M. Sarikaya, and D. M. Dabbs

13a. TYPE OF REPORT	13b. TIME COVERED	14. DATE OF REPORT (yr., mo., day)	15. PAGE COUNT
Final	FROM 901001 TO 921231	930928	33

16 SUPPLEMENTARY NOTATION
AFOSR-91-0040

COSATI CODES		
FIELD	GROUP	SUB. GR.

18. SUBJECT TERMS (Continue on reverse if necessary and identify by block number)
nanodesigned multifunctional ceramics
ceramic processing
colloidal processing

19. ABSTRACT (Continue on reverse if necessary and identify by block number)

Methods of processing nanometer scale ceramics for use in structural and optoelectronic applications have been developed. Colloidal processing of fine scale ceramic powders was used because such an approach represents the most feasible processing methodology for the production of large scale devices and components. The project consists of two primary task areas: (i) fundamental studies in synthesis and processing and (ii) the processing and properties of ceramic matrix composite. For task one, the emphasis has been on the basic science of the synthesis and use of nanometer size particles. Task two, on the other hand, has been on the application of colloidal methods to the production of ceramic matrix composites for use in engineering applications.

This project began at the University of Washington and was continued at Princeton University.

20. DISTRIBUTION/AVAILABILITY OF ABSTRACT	21. ABSTRACT SECURITY CLASSIFICATION
APPROVED FOR PUBLIC RELEASE: DISTRIBUTION UNLIMITED	UNCLASSIFIED

22a. NAME OF RESPONSIBLE INDIVIDUAL	22b. TELEPHONE NUMBER (Include Area Code)	22c. OFFICE SYMBOL
Major Thomas E. Erstfeld, USAF	(202) 767-4960	NC

FORM 1473, 83 APR — EDITION OF 1 JAN 73 IS OBSOLETE.

SECURITY CLASSIFICATION OF THIS PAGE

Nanodesigning Of Hierarchical Multifunctional Ceramics

Air Force Office of Scientific Research
Final Technical Report for Grant No. AFOSR-91-0040

I. A. Aksay, Principal Investigator

February 28, 1993

Department of Chemical Engineering and
Princeton Materials Institute

Princeton University
Princeton, New Jersey 08544-5263

Table of Contents

List of Figures

NANODESIGNING OF HIERARCHICAL MULTIFUNCTIONAL CERAMICS

Ilhan A. Aksay

Executive Summary

The project entitled "Nanodesigning of Hierarchical Multifunctional Ceramics" (Grant No. AFOSR-91-0040) began October 1, 1990, and extends the work done within the "Microdesigning of Lightweight/High Strength Ceramic Materials" projects from 1983 through 1990. The research on lightweight/high strength ceramic materials was jointly supported by the Air Force Office of Scientific Research and the Defense Advanced Research Projects Agency (Grant Nos. AFOSR-83-0375, 1 October 1983 to 30 November 1986, and AFOSR-87-0114, 1 December 1986 to 28 February 1991). This report is the final technical report for the most recent project, covering the period October 1, 1990, through December 31, 1992.

The principal focus of our earlier projects under AFOSR sponsorship from 1983 to 1991 was to establish guidelines for processing low density (< 3.0 g/cc) and high strength (> 800 MPa) ceramic matrix composite materials for structural applications. The achievements of the first six years of the research program have led to the development of improved ceramic fabrication processes mainly with the use of colloidal dispersion and consolidation methods. Fundamental issues on the dispersion of mainly micron-sized powders with polymeric processing aids, the consolidation methods, and microstructure evolution in single and multiphase systems were addressed both experimentally and theoretically. However, for all the answers provided, additional questions were raised indicating a new direction focused on the length scale of 1 to 100 nm where our knowledge of materials synthesis and processing by deliberate design appears to be the weakest. Since this is also the range where phenomena associated with atomic and molecular interactions strongly influence the macroscopic properties of materials, the main focus of our projects shifted to the issues related to the ***nanodesigning*** of ceramic matrix composites with the use of colloidal dispersions and molecular precursors.

The concept of ***hierarchy*** relates to the fact that macroscopic properties are not just influenced by the phenomena associated with one length scale but are determined by the accumulation of "substructural" properties at various length scales originating from atomic to microscopic dimensions depending on the structural features of aggregation. In order to design materials with predictable properties, structural development has to be closely controlled at each step during processing, beginning with mixing (at the nanometer scale) and continuing through the densification of the constituent phases (at the micron and larger scales). For instance, in the design of an electrochromic display device as a ***multifunctional*** ceramic material, an architectural hierarchy of layering in an electrochromic ceramic with a conductive polymeric phase becomes essential at micron and larger length scales. Similarly, thin (< 1 μm) films of ceramic ferroelectrics are of interest for numerous microelectronic applications including non-volatile memories, piezoelectric microsensors and actuators, optical memories, and dielectric layers. However, the successful utilization of these ferroelectrics requires not only a fundamental understanding of synthesis and processing at nanometer length scale but also their incorporation into hierarchically architectured devices at larger length scales at sufficiently low enough

temperatures so that the direct-gap semiconducting substrates (e.g., GaAs) will not lose their intrinsic properties.

The research projects summarized in the following sections were all selected to meet this end goal of designing multifunctional ceramics for structural, electronic, and optical applications with a starting point at the atomic and nanometer level. Our choice of a colloidal approach to processing stems from the recognition that for the production of large scale devices and components, this will be the most feasible approach. The projects are categorized into two task areas as: (i) fundamental studies in synthesis and processing and (ii) processing and properties of ceramic matrix composites. In the first task area the research projects are concerned primarily with the basic science of the synthesis of nanometer-sized particles and nanodesigning through the use of colloidal suspensions. In the second task area the key emphasis is on the application of fundamental concepts generated in our previous projects to produce novel composites that can be utilized in engineering applications.

Technical Report

1. Fundamental Studies in Synthesis and Processing

This portion of our research project is concerned primarily with the basic science issues on the processing and characterization of multifunctional ceramics with deliberately introduced features ranging from microscopic to macroscopic dimensions. The primary goal of most of the projects is on the issues related to *nanodesigning* since this is the area where our basic knowledge is the weakest. Projects are discussed within two subtasks: (i) synthesis of nanometer-sized particles and colloidal suspensions and (ii) consolidation and densification of nanometer-sized particles.

1.1 Synthesis of Nanometer-sized Particles and Colloidal Suspensions

Studies on the synthesis and stabilization of nanometer-sized colloidal gold date back to Faraday's pioneering work that is more than a century old. In our past studies, we used colloidal gold particles of ~ 15 nm in diameter to determine the conditions that result in ordered arrangement of the particles versus fractal aggregates. In our most recent studies, we have concentrated on the mechanisms that result in the formation of these particles with a very narrow particle size distribution in a size range that is of interest in various emerging applications ranging from the synthesis of quantum dots (e.g., GaAs) by colloidal methods to the processing of nanocomposites for structural applications. As explained below, our work has now resulted in a satisfactory explanation for the formation of these nanometer sized particles with a very narrow size distribution.

1.1.1 Formation of Nanometer-sized Gold Particles

Investigators: J. Liu, W. Y. Shih, W.-H. Shih, M. Sarikaya, and I. A. Aksay

Although the synthesis of nanometer-sized gold colloids is well documented in most colloid textbooks,[1] the homogeneous nucleation and growth mechanism which has been used to explain the formation of these particles conflicts with the observed color change during the synthesis stages. As shown in Fig. 1, during the preparation of the colloidal gold, the solution first appears greyish blue (Fig. 1(b)) before it turns ruby color at the end (Fig. 1(f)). With the known dependence of the color of gold colloid on particle size, this observation on the color change implies that gold particles reduce their size at the final stage of the growth process, a phenomenon which contradicts the traditional view of nucleation and growth, i.e., once nuclei form, average particle size increases monotonically.

In our experiments, colloidal gold was produced by reducing gold chloride with sodium citrate in dilute aqueous solution. Morphological changes of the particles and their clusters were examined by transmission electron microscopy using a technique described elsewhere. In parallel, the electrophoretic mobility of the particles was measured by Döppler elastic light scattering, and the optical transmittance was monitored by UV transmittance spectrometry. These studies provided the following information on the formation of particles corresponding to the stages indicated in Fig. 1: (i) First, nuclei (or primary particles) of about 2-4 nm in diameter formed and aggregated by diffusion-limited aggregation as the color of the suspension changed from white to greyish blue; (ii) Next, after these aggregates reached a maximum size, restructuring and breakup of clusters started accompanied by a developing charge on the particles; (iii) Finally, the particles reached approximately the same ultimate size and the suspension became ruby colored. This sequence, which differs from the traditional homogeneous nucleation and growth process,

explains the unusual color change observed during the formation of the particles. In the initial stage aggregation is due to the van der Waals attraction between the particles, and the restructuring and breakup is a result of the charge buildup during the reaction process. Based on a model that we are developing, the breakup and the formation of the monodispersed particles is realized through interfacial energy minimization when particles develop a surface charge. The experimental results on the dependence of particle size on citric acid concentration and the standard deviation as a function of particle size agree well with our theoretical prediction based upon the principle of energy minimization (Fig. 2).

Although presently we do not yet understand the exact nature of the surface charge dependence on the citric acid concentration, this study provides a new insight into nanometer-sized colloidal particle formation. As shown below, we are now in the process of extending these model studies to interpret reversible color changes observed in electrochromic ceramic suspensions and gels (Section 1.1.2) and the formation of monosized dielectric $BaTiO_3$ particles (Section 1.1.3) and thin films that we intend to use in designing of multifunctional ceramic composites (Section 1.2.7).

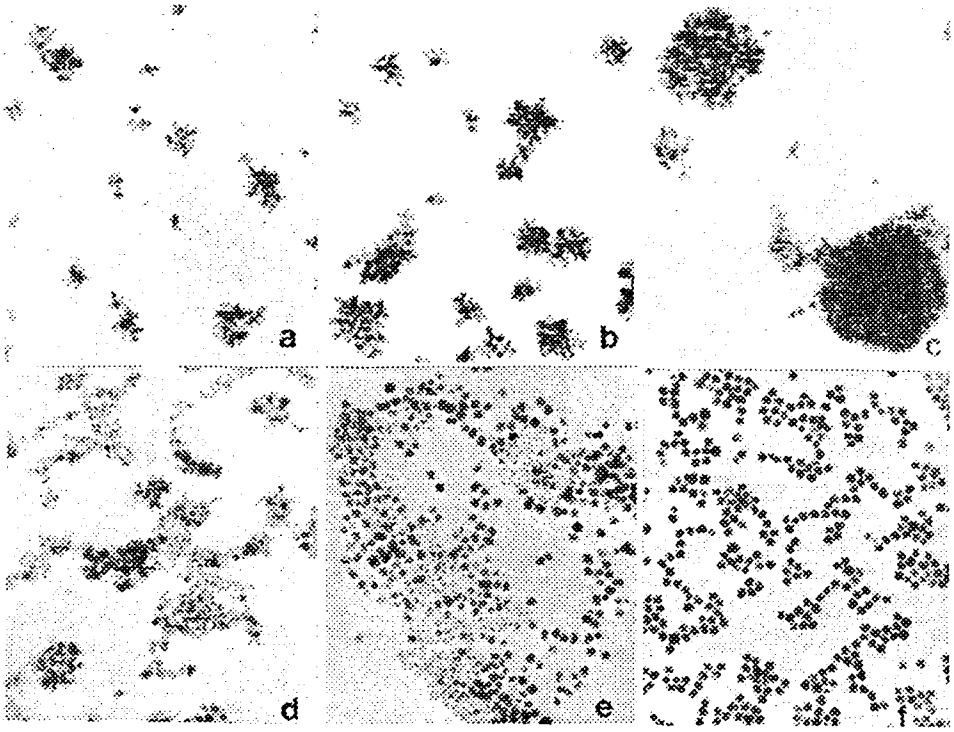

Figure 1: Color changes during the nucleation and growth of colloidal gold in a gold chloride solution relate to the clustering of primary particles. The color changes from white (Fig. 1(a)) to a grayish blue (Fig. 1(c)) prior to the final ruby color (Fig. 1(f)).

1.1.2 Electrochromic Colloids and Gels

Investigators: G. Magendanz, J. Liu, M. Sarikaya, and I. A. Aksay

Electrochromic materials have been extensively studied for use in information display, automotive applications, and energy efficient windows. Electrochromism is a reversible color change in a material caused by an applied electric field or current. Many organic and inorganic materials exhibit electrochromic behavior, including several transition metal oxides. The most

widely studied is tungsten trioxide, WO_3. Devices utilizing these materials could be designed for numerous applications. For example, a glass whose light transmission can be actively controlled would represent a significant addition to the arsenal of materials for energy efficient building construction.

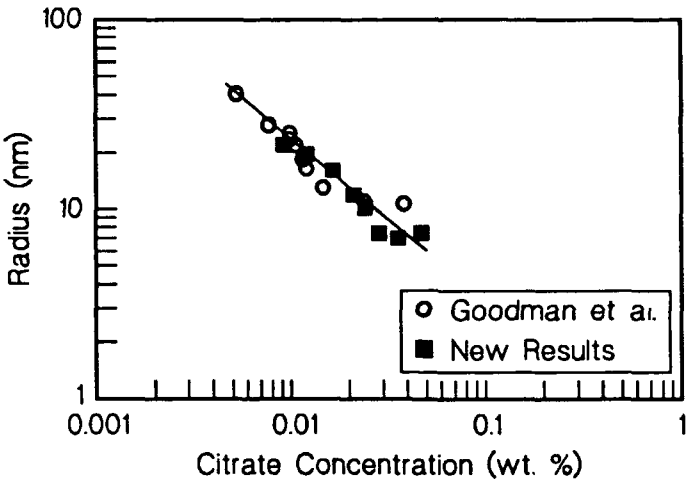

Figure 2: The observed dependence of the colloidal gold particle size on the concentration of the citrate ion in solution.

Our interest in electrochromic ceramic suspensions and gels stems from the need to identify materials that can be used in an interactive mode in designing of multifunctional materials. For practical applications, electrochromic devices are constructed so that electrical current can pass through the material causing the color change. A hierarchically arranged sandwich configuration allows a reversible chemical reaction to cycle metal ions between the electrochromic material and an ion storage media. The generally accepted electrocoloration mechanism involves the simultaneous double injection of ions and electrons into WO_3 to form a bronze:

$$WO_3 + xM^+ + xe^- \rightarrow M_xWO_3 \qquad (1)$$

However, our preliminary experiments indicated that color change in these systems may not be entirely associated with the valance changes but may also relate to the morphological changes of the particles and their clusters (Section 1.1.1). As shown in Fig. 3, during the application of an electrical field we observe a significant volume change in the suspension. This suggests that a network rearrangement is taking place as the color of a WO_3 suspension changes from white to light blue and finally to dark blue. Our objective in this study has been to separate the contribution of the morphological changes from any valance effects. We envision that these morphological changes will also relate to the lifetime of electrochromic devices since physical changes in the gel system may hinder color reversibility and lead to device degradation.

In our experiments hydrated tungsten oxide is produced by the acidification of an aqueous sodium tungstate solution. The precipitated tungstate is then used to analyze possible physical changes associated with the color change of the tungsten oxide. The color change, white to blue, is obtained by UV illumination or by application of an electric current. We are presently exploring the physical characteristics of a tungstic gel by transmission electron microscopy as its color is changed in an electrochemical cell. To date gels have been used for bulk color reversibility studies, UV/Visible spectroscopy, cyclic voltammetry, and thin film spinning. Future work

includes the development of a non-aqueous electrochemical cell for thin film coloration. Electron microscopy will require the fabrication of a thin film on a TEM grid so that morphology can be examined at varying stages of coloration. Light scattering and studies of film degradation as a function of the number of times the film has been cycled are planned for a subsequent phase to this project.

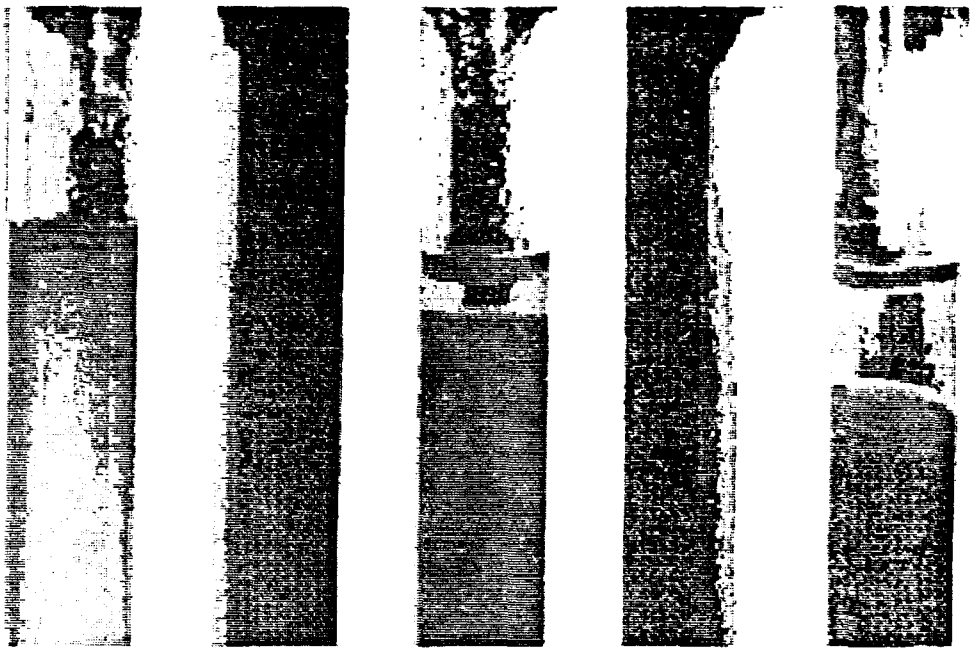

Figure 3: Electrocoloration in WO_3 gels is associated with a significant change in the volume of the gel. This suggests that the gel network has rearranged during the color changes.

1.1.3 Nucleation and Growth of Nanometer-sized Barium Titanate Particles

Investigators: F. Dogan, C. Chun, J. Liu, M. Sarikaya, and I. A. Aksay

Barium titanate powder is conventionally prepared by the reaction of mixed powders of TiO_2 and $BaCO_3$. These powders have relatively large particles (> 1 μm) which are agglomerated and have a wide size distribution. In contrast, recent studies have shown that submicron and nearly monosized $BaTiO_3$ can be prepared under hydrothermal conditions by reacting nanosized titanium oxide or titanium alkoxides with a solution of barium hydroxide. The powders produced by this approach range in size from an apparent lower limit of 0.1 μm up to several microns in diameter. Presently, the mechanisms leading to formation of these particles with a lower limit of 0.1 μm are not understood.

As in the formation of nanosized gold particles (Section 1.1.1), the goal of this study is to determine the parameters that control the ultimate particle size and the morphology of $BaTiO_3$ particles. If the particle size can be reduced below 0.1 μm, these particles can be used in a variety of applications ranging from the sintering of transparent polycrystalline $BaTiO_3$ to the processing of nonlinear optical ceramic-polymer composites using colloidal dispersion techniques.

In our experiments, we used either a high purity titania sood or titanium isopropoxide mixed with a clear solution of 1M $Ba(OH)_2$ $8H_2O$ at a Ti:Ba ratio of 1:1.1. The reaction was conducted at 80°C in sealed polyethylene bottles without stirring. In order to study the extent of reaction, samples were taken from the suspensions at different times between 10 minutes and 48 hours.

Each suspension was washed by centrifugation using CO_2-free water to remove unreacted $Ba(OH)_2$. Washing was carried out at room temperature to prevent leaching of Ba^{2+} ions from $BaTiO_3$ particles. TEM characterization was conducted using EELS and EDS for compositional analysis. The phase transformations were determined by XRD. As in previous studies, the final particle size of $BaTiO_3$, obtained from either the titanium isopropoxide solution or the titania powder, was around 0.1 μm indicating that the particle size is not affected by the source of the titania precursor. However, by increasing the size of the initial titania particles, the size of $BaTiO_3$ particles was also increased.

At the initial stage of development, the surfaces of the barium titanate particles were observed to be faceted; HREM images revealed that these particles are single crystals. After the reaction was completed (after 48 hours), the particle surfaces were smoothed and the particles became spherical. These results suggest that the particles are not formed by the direct reaction of colloidal titania particles and the barium ions in the solution through a diffusion mechanism as proposed in previous studies. Instead, the $BaTiO_3$ particles are formed directly from the solution, as in the specific case of gold colloid formation discussed in Section 1.1.1. Therefore, as in the case of gold particle formation (Fig. 2), we expect the surface charge characteristics of the particles to be a key determinant on the ultimate size of the produced particles.

1.1.4 High Resolution Structural Characterization of Electronic Ceramics

Investigators: T. Yoshimori, K. Sastry, M. Qian, M. Sarikaya, and I. A. Aksay

In this portion of the project we focused our efforts in two areas: (i) the development of high spatial resolution electron spectroscopy, namely, electron energy loss spectroscopy, and (ii) the structural characterization of electronic ceramics using advanced microscopy techniques.

Development of High Spatial Resolution Spectroscopy:

It is well-known that the EELS technique has great potential in analyzing quantitative concentrations for all elements from hydrogen to uranium as well as spectroscopy in the region from 0 to 2000 eV. For example, various prominent features of the EELS spectrum are used for spectroscopic analyses: oxidation states, dielectric constant determinations, binding energies, and short range ordering. Our objective has been to develop a new scheme for the acquisition of electron energy loss spectra and to improve the spectroscopic data analysis capabilities of this technique.

It is difficult, in general, to perform quantitative EELS to determine relative or absolute compositions of elements with relatively high atomic numbers, to use ELNES (energy loss near edge structure) to determine oxidation states, or to determine short range ordering by use of EXELFS (extended energy loss fine structure). In all of these cases it is essential to have a high signal-to-noise ratio and sufficient energy resolution (~1 eV), requirements which are, in general, difficult to attain. There are three inherent limitations in spectrum acquisition using EELS in a TEM. These are: (i) the large intrinsic background found in EELS spectra, (ii) the channel-to-channel gain variation (CCGV) in the parallel detection system, and (iii) difficulties in obtaining statistically high total counts (~10^6) per channel. The last two limitations may be circumvented and the signal to noise ratio may be improved by improving on-line data acquisition procedures.

EXELFS (extended energy loss fine structure) spectroscopy contains unique information of local atomic structure, same as XAFS (X-ray fine structure), but has several advantages over XAFS, such as having high spatial resolution (nanoscale versus bulk), better low Z element sensitivity, parallel detectability, and no dependability on synchrotron-radiation-sources. Due to

poor statistical total counts, however, EELS data quality is inferior and, therefore, EXELFS technique has not been well developed to its full advantages. The main limitations in EELS acquisition are channel-to-channel gain variations (CCGV) in the parallel detection system and low S/N ratio due to the instability of instrument that prevents long acquisition times. Techniques that circumvent CCGV, such as first or second difference, do not allow the retrieval of EXELFS signal from the spectra. Recently we have improved the EELS data acquisition technique so that CCGV could effectively be corrected and statistical fluctuations could reach a level much lower than that in the fine structure. These improvements have opened up the possibility of deducing accurate atomic structure information from EELS spectrum at relatively high energy values (1000 to 2000 eV).

Nb Distribution and Its Effect on Properties of $BaTiO_3$:

A small amount of a dopant added to a perovskite material used as a dielectric greatly influences its properties. Dopants are added to materials to modify properties but there is a lack of detailed investigation on the effect of dopants on the lattice structure, valance states, bonding, and resultant electronic properties. For example, the addition of Nb (0.2 to 0.9 % of Ti) affects the electronic and structural properties of $BaTiO_3$ but it has not yet been possible to determine the location and distribution of Nb in the lattice and the structure of $BaTiO_3$ after doping. Our objective is to quantitatively determine the amount of Nb in the structure, its distribution and location in the perovskite lattice, and its effect on the electronic properties. This type of study requires high spatial resolution analysis, simultaneously using a spectroscopic technique that probes both energy shifts as a result of the doping and the amount of compositional variations at the nanometer scale). Consequently, we began our study using a high resolution transmission electron microscope (TEM) fitted with nanometer-sized electron probes and a parallel detection electron energy loss spectrometer (EELS).

The investigation consists of three related projects, all using the same EELS spectra. These are: (i) the quantitative analysis of the Nb concentration in insulating and semiconducting portions of the doped-sample; (ii) determination of Ti/O and Ba/Ti ratios in the presence and absence of Nb; and (iii) a possible change in the oxidation states of Ti and Ba in the presence of Nb, studied by extended energy loss fine structure analysis (ELNES). Since data acquisition must be done without damage to the sample a low temperature holder is used that keeps the sample temperature at ~ −165°C.

In order to determine quantitatively the amount of Nb in the lattice, EELS spectra were taken with energies between 65 eV through 565 eV. This window includes Ba-N_4, $NbM_{4,5}$, Ti-$L_{2,3}$, and O-K edges. The aim is to calculate the absolute value of the number of Nb atoms under the N_4 edge in the doped sample. This can theoretically be determined by taking two spectra, one from the doped sample, and the other from a standard $BaTiO_3$ sample. Although there is a "hump" in the spectrum from the Nb-doped sample, its position does not match that of any of the possible Nb-N edges. In addition to these, first and second difference spectra did not produce any conclusive results up to this point.

Given that the formula for the complete doping is $BaTi_{1-x}Nb_xO_3$, addition of Nb should result in an overall compositional change in the lattice. Since compositions down to 0.01% can be determined in EELS provided that there is a sufficient signal, using the Ba-N_4, Ti-$L_{2,3}$ and O-K edges from standard and doped samples, one should be able to determine these variations. In spectra taken at a thickness of about 0.3 times the mean-free-path thickness (about 200 Å), there is definitely a difference in the Ba/Ti, Ba/O, and Ti/O ratios. There are a number of possible

stoichiometries calculated from these ratios based on the valent state of the titanium in the perovskite structure. Work is now proceeding in an attempt to determine the valent state(s) of the titanium in Nb-doped barium titanate.

1.1.5 Processing of Ceramic Fibers from Particle Suspensions

Investigators: W. M. Carty and I. A. Aksay

During the past thirty years, the development of polycrystalline ceramic fibers has lead to significant advances in high temperature composites. Other potential applications include piezoelectric sensors and high efficiency transmission lines composed of high-temperature superconductors. Yet, unless the fiber is formed from a homogeneous glass melt, the composition range of the ceramic fibers is limited to spinnable inorganic polymeric precursors. The ability to form spinnable inorganic polymeric liquids is then limited to the range of compositions (e.g., silicon, carbon, nitrogen, and aluminum based systems) for which the problems associated with chemical synthesis have already been solved. Further, these methods frequently rely on the use of organic solvents, which create potential health and safety problems.

In order to minimize the problems associated with chemical synthesis and thus to establish a more robust procedure for fiber processing, we have initiated this study on the preparation of ceramic fibers from aqueous suspensions of colloidal particles. The goals of this research are: (i) to develop an understanding of what limits or controls spinnability and (ii) to compare fibers prepared using this method to commercially available alumina fibers. The final stage of the project will be to check the concept of suspension spinning on a different system, such as that of the piezoelectric ceramic $Pb(Zr_{0.52}Ti_{0.48})O_3$ (PZT).

Our initial work centered on the processing of alumina fibers, but, hypothetically, the process should be applicable to any system in which stable aqueous suspensions can be prepared. The experimental results thus far indicate that it should be possible to form fibers from any aqueous particle suspension. Fibers were spun from aqueous suspensions of α-Al_2O_3 to which high molecular weight poly(ethylene oxide) was added. From observation of the spinning experiments, a process map (Fig. 4) was constructed which identified spinnable compositions. From these results, the fluid properties necessary to allow spinnability were qualitatively identified.

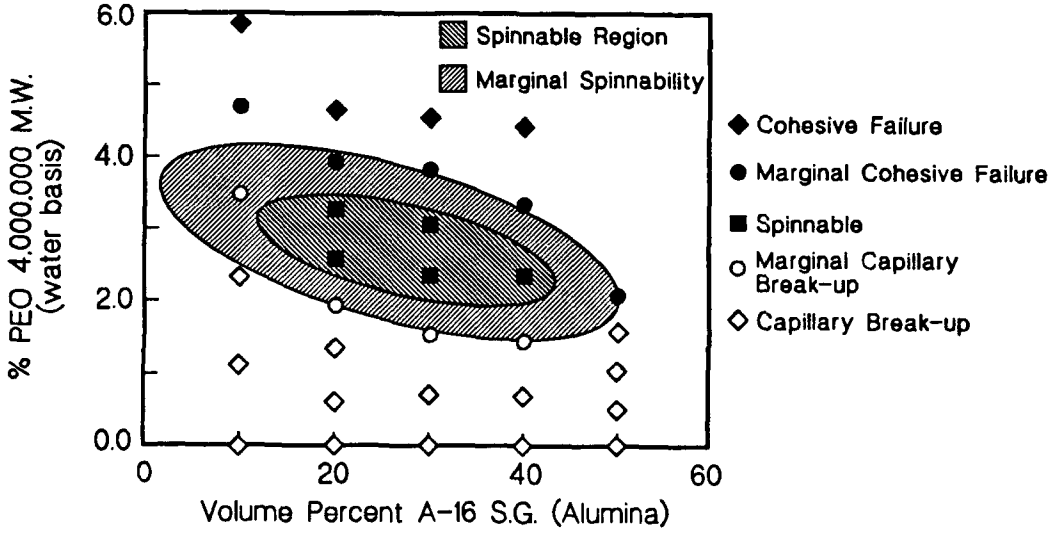

Figure 4: Spinnability map for poly(ethylene oxide)-based α-Al_2O_3 suspensions.

1.2 Consolidation and Densification of Nanometer-sized Particles

Nanometer-sized particles and the nanocomposites produced with these particles display unique physical properties. However, various synthesis and processing problems severely limit the development of these composites in commercial applications. In Sections 1.1.1 to 1.1.3, we addressed some of the issues on the synthesis of nanometer-sized particles. Issues related to dispersion and consolidation were addressed in our previous studies. As an extension of these studies, in the following sections, we now address some of the key issues on the densification of compacts produced with these particles.

One of the major problems in processing nanostructured materials is their tendency to coarsen rapidly as grain growth dominates at elevated temperatures. Consequently, the unique properties that are observed at low temperatures disappear at elevated temperatures. One successful approach to enhance the high temperature stability of these composites against grain coarsening is through the entrapment of second phase particles within the grains of a matrix phase so that diffusional distances to the grain boundaries can be increased and thus the processes of coarsening can be slowed down kinetically. Towards this goal, in Section 1.2.1, we examine the densification of nanosized gold particles in order to establish a base line for the densification and grain growth processes in single phase nanostructured materials. In Section 1.2.2, we summarize the results of computer simulation on the densification of nanosized particles. Experimental results on the processing of lead zirconium titanate and barium titanate ceramics at temperatures as low as 450°C and 80°C, respectively, are reported in Sections 1.2.3 to 1.2.5.

1.2.1 Structural Evolution During Sintering of Nanometer-sized Particles

Investigators: J. Liu, M. Sarikaya, and I. A. Aksay

The objective of this study has been to determine the mechanisms of densification and grain growth of nanometer-sized particle by an in-situ transmission electron microscopy technique. As a model system, we again used colloidal gold particles because of their high atomic scattering factor, which is helpful for electron diffraction and imaging. Since the formation of colloidal gold is well understood, the particle size and shape can be easily modified. Our previous studies have shown that nanometer-sized particles can be arranged in different configurations through colloidal techniques by controlling the interfaces between the particles as well as the particle interaction energies. Direct TEM observations on these model packings then provides an opportunity to develop models on the sintering mechanisms in nanostructured materials. The results of our recent studies are summarized as follows:

(i) The shape of the particles is not stable. The instability may come from the local energy minima between different shapes. This implies that the particles can deform more easily than large particles. When sintering occurs under heating, the particles can also deform due to the stress gradient, therefore accelerating the sintering process.

(ii) Room-temperature sintering occurs for nanometer-sized particles. When particles touch one another, a neck forms between the particles even without heating. This shows that sintering will occur at a much lower temperature compared to large particles.

(iii) Diffuse grain boundaries were observed between the particles. The crystalline structure continues from one particle to another, and there is not a clear interface between the particles (Fig. 5). Yet a sharp grain boundary is usually observed between large particles. When these large particles are heated, grain growth occurs. A sharp grain boundary appears when the particles grow to a larger size. Since grain boundary diffusion is one of the most important

processes for densification, a diffuse grain boundary implies that the sintering of nanometer-sized particles will follow a behavior different from that of large particles.

(iv) When sintering takes place, a considerable lattice structure change occurs in the grain boundary region as well as within the particles. This indicates that rearrangement takes place by a cooperative motion of the atoms. In contrast, with particles >1 μm, only diffusional deformation is observed at the grain boundaries (Fig. 5).

(v) In order to better understand the sintering process, the particles arranged in a chain configuration were heated under constant electron beam intensity to mimic a constant temperature sintering process, and electron microscope images were recorded at different times. The neck sizes between the particles were measured from the photographs taken at different times. Then the neck sizes were plotted as a function of time at the initial sintering stage on a log-log scale (Fig. 6). During the initial sintering stage, the neck size is usually related to time by a power-law relationships, and the power is indicative of the sintering mechanism. When the experimental results were compared with the predictions from the sintering models based on diffusion, the power is much too high. In fact, the power obtained from our experiments was 0.5. Only viscous sintering will give a power of 0.5. Therefore it can be concluded that the sintering of nanometer-sized particles differs from that of large crystalline particles, which only involves diffusion. It is possible that the cooperative motion of the atoms in nanometer-sized particles is similar to viscous sintering of amorphous materials.

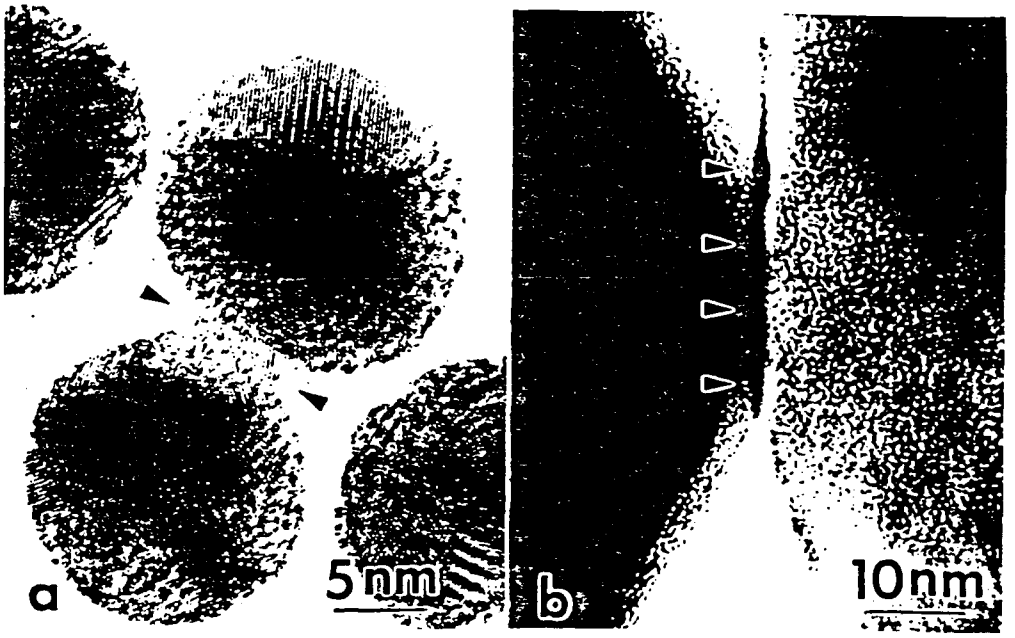

Figure 5: High resolution electron microscope images of the particle to particle contact regions in (a) nanometer-size colloidal gold suspensions and in (b) micrometer-size gold particle suspensions.

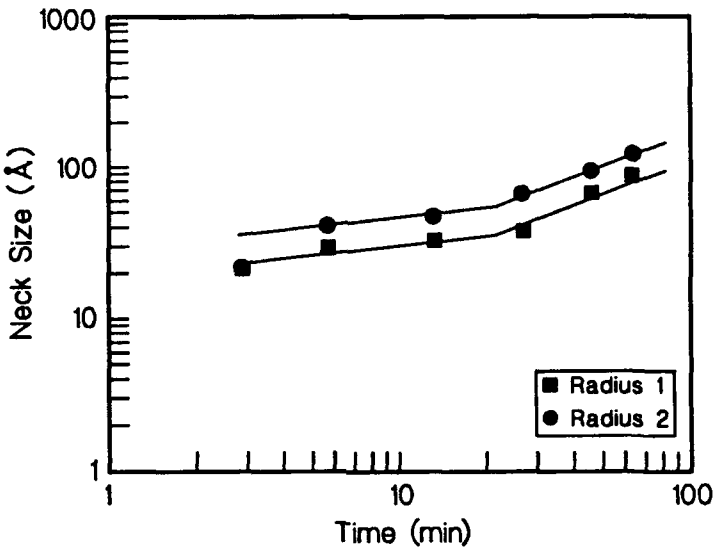

Figure 6: The variation in the neck size is a function of time in the sintering of nanometer-size colloidal gold particles.

In summary, the sintering of nanosized particles is different from that of large crystalline particles. Due to the diffuse grain boundaries and collective motion of atoms, which is similar to plastic deformation, sintering is much faster than that predicted by the diffusion law. Further study will focus on the exact mechanisms of the plastic deformation process. Theoretical study is also needed to understand the behavior of a system of a finite size in which the atomic periodicity is truncated to a low dimension. Modeling of the cooperative behavior of multiparticle systems is also necessary. The experimental problems that need to be solved are: the effect of the substrate, the effect of contamination from the non-ultrahigh vacuum environment, the effect of electronic interaction as compared with thermal heating, and the universality problem. It may be necessary to use a microscope with a hot stage in ultrahigh vacuum. Other materials and different substrates will also be studied.

1.2.2 Sintering of an Isolated Pore

Investigators: W. Y. Shih, W.-H. Shih, and I. A. Aksay

In our previous work, we studied the sintering behavior of an isolated pore in a polycrystalline matrix using Monte Carlo simulations. The simulations were done in two dimensions. The main results of the Monte Carlo simulations were: (i) grain growth slows the sintering rate; (ii) when the average grain size is kept fixed and the sample size scales proportionally to the pore size, the pore elimination time t scales with the initial pore radius r as $t \sim r^4$ for small pores and as $t \sim r^3$ for large pores; (iii) for a fixed sample size much larger than the pore size, the pore elimination time t scales with the pore size r as $t \sim r^3$ for small pores and $t \sim r^4$ for large pores; and (iv) the crossover from the small-pore scaling to the large-pore scaling occurs at a larger pore size when the average grain size is increased. At the start of this project our goal was to explain the scaling behaviors observed in our simulations.

Assuming that the transport channels are the grain boundaries, we were able to develop a scaling theory using arguments similar to that of Herring to account for the various scaling laws

obtained in our simulations. We found that the total cross sectional area S of the grain boundaries intersecting the pore surface is given by two relationships:

$$S \sim \frac{r^{d-1}}{G} \qquad \text{for pores larger than the grain size } G;$$

and

$$S \sim r^{d-2} \qquad \text{for pores smaller than the grain size } G.$$

These relationships have been found to be consistent with our simulation results. Thus, the difference in the total cross sectional area of the grain boundaries intersecting the pore surface gives rise to the different scaling behavior observed between large and small pores. The scaling theory also indicates that the relationships between the pore elimination time and the pore radius as defined above are independent of the dimension; therefore, our two dimensional simulations hold for three dimensions. A manuscript describing this work has been prepared for submission to the *Journal of the Materials Research Society.*

1.2.3 Density-pressure Relationship of Boehmite Suspensions and Alumina Suspensions in Pressure Filtration and Centrifugation

Investigators: Wei-Heng Shih, S. I. Shih, Wan Y. Shih, and I. A. Aksay

Both dispersed and flocculated alumina suspensions have been studied with pressure filtration. In the case of dispersed alumina cakes, the final cake density is known to be independent of the applied pressure whereas in flocculated alumina suspensions the cake density increases logarithmically with pressure. The goal of this portion of the project is to compare the consolidation behavior of nanometer-sized boehmite suspensions under pressure filtration with the behavior of alumina suspensions and to explain the consolidation behavior of both alumina suspensions and boehmite suspensions under centrifugation..

We have found that the pressure filtration behavior of boehmite suspensions is similar to that of alumina suspensions; i.e., the final cake density of boehmite suspensions increases logarithmically with the applied pressure. However, the density of the boehmite cakes are much smaller than that of the alumina cakes under the same consolidation pressure. We have determined that the logarithmic relationship between the final cake density and the applied pressure is a result of the restructuring of the particulate network. The final cake density of dispersed boehmite suspensions also increases logarithmically with applied pressure but is lower than cake densities from pressure-filtered alumina suspensions, indicating that aggregation is inevitable with nanometer-sized boehmite particles even in a seemingly dispersed suspension. This result implies that for dispersed or flocculated boehmite suspensions pressure filtration is an effective consolidation technique. For a flocculated boehmite suspension with a 5 vol% initial density, the dried cake density was 52.5 vol% which is very impressive for the nanometer sized boehmite particles.

At low densities, the pressure of boehmite suspensions are orders-of magnitude higher that those of alumina suspensions. However, the extrapolated pressure of flocculated boehmite suspensions at 65 vol% is only about twice that of alumina suspensions at the same density due to a smaller slope of density-vs.-log (pressure). This further indicates that pressure filtration is effective for consolidating nanometer sized boehmite particles. We also found that the final cake density increases strongly with the increasing initial particle density, indicating that changing the initial particle density is more effective in improving the packing density than changing the

suspension pH. In contrast to pressure filtration, centrifugation of boehmite suspensions shows a power-law dependence of the final cake density on the mean applied pressure, indicating that the flocs still retain their fractal nature after they pack to form the cake. A manuscript has been prepared for submission to the *Journal of the American Ceramic Society.*

1.2.4 Equilibrium-State Density Profiles of Centrifuged Cakes

Investigators: Wei-Heng Shih, Wan Y. Shih, Seong-Il Kim, and Ilhan A. Aksay

We have shown previously that the mean pressure $P_{s,m}$ of a centrifuged cake of a flocculated suspension is related to the average cake density ϕ_{ave} as:

$$P_{s,m} = \beta \phi_{ave}^{n} , \tag{1}$$

where the coefficient β and the exponent n depend on the suspension pH, the materials, the particle size, and also the initial suspension density. The exponent n increases as the degree of flocculation decreases, or as the density increases. Meanwhile, density profiles of centrifuged cakes of flocculated alumina suspensions and those of flocculated boehmite suspensions have been examined experimentally with γ-ray densitometry. We showed that as the suspensions become more strongly flocculated, i.e., the exponent n becomes smaller, the density variation in the centrifuged cakes becomes more severe. Our objective in this work is to develop an analytic theory that will allow us to understand the cause of the density variations that occur in centrifuged cakes. This kind of understanding is crucial to improve the density uniformity of centrifuged cakes.

Our theory was developed by implementing the experimental pressure-density relationship depicted in Eq. (1) into the general differential equation for centrifugation *with appropriate boundary conditions*. Previously, we did not incorporate the boundary conditions in the calculation. As a result, we could not predict the density variations near the cake-supernatant interface. In the present work, we also take into account that the cake density near the cake-supernatant interface and that the total accumulative density of the cake is the same as that of the initial suspension, i.e.,

$$\phi(z_m) = 0, \tag{2}$$

and

$$\int_{r_c}^{z_m} \phi(z)\, dz = \phi_0 h_0 \tag{3}$$

Here z is the distance from the bottom of the cake, z_m the distance at which the cake density vanishes and ϕ_0 and h_0 are the density and the height of the initial suspension, respectively. By doing so, we are able to solve for the entire density profile.

Furthermore, we show that the density profile $\phi(z)$ of a centrifuged cake of a flocculated suspension can be approximated in a universal form as

$$\frac{\phi(z)}{\phi_{max}} = \left(1 - \frac{z}{z_m}\right)^{\frac{1}{n-1}} \tag{4}$$

where ϕ_{max} is the maximum density at the bottom of the cake. Thus, one can immediately see that the relative density variation within the cake increases as n decreases. The experimental

results were in good agreement with this prediction. For the same suspension conditions, i.e., with the same n , ϕ_{max} increases and, therefore, z_m decreases with an increasing centrifugation frequency ω. As a result of the universal dependence of the relative density on z/z_m, the density gradient actually increases with an increasing ω despite the increase in the average cake density. Equation (4) can also be used to describe the density profiles of a sedimented cake provided that the pressure-density relationship of a sedimented cake is also a power-law function $P = \beta\phi^n$.

While the $(1-\frac{z}{z_m})^{\frac{1}{n-1}}$ dependence of the relative density is an approximation for centrifuged cakes, it is exact for sedimented cakes. The relative pressure can be expressed as

$$\frac{P(z)}{P_{max}} = (1 - \frac{z}{z_m})^{\frac{n}{n-1}}. \qquad (5)$$

The uniform density profiles observed in the sedimented cakes of disperse suspensions[2,3] can also fit the form of equation (4) as explained below. The cake density of dispersed suspensions has been shown to be independent of the applied pressure.[4,5] The independence of the cake density with respect to the pressure means that n is very large if $P = \beta\phi^n$ is used to describe the pressure-density curve. The large n value gives negligible $1/(n-1)$ values, therefore, negligible density variations in the main portion of the cake are observed in the density-profile measurements.

Finally, in the case of strongly flocculated cakes, especially, the ones formed by nanometer-sized particles such as boehmite at pH = 5.5, the viscoelasticity of such cakes will allow the cakes to spring back significantly. The springback of the cake may give rise to non-monotonic density profiles. The density profiles after significant springback is not within the scope of the present paper. The monotonic density profiles predicted by Eqn. (4) is good for cakes that are immediately removed from the centrifugation unit as we have done in the experiment or cakes that do not have significant springback such as alumina at pH = 7.0 or boehmite at pH = 7.0. A Materials-Research-Society (MRS) proceeding paper has been accepted for publication on this work and a manuscript has been written to be submitted for publication in the *Journal of American Ceramic Society*.

1.2.5 Density of Colloidal Aggregated Network Near a Hard Wall

Investigators: W. Y. Shih, W.-H. Shih, and I. A. Aksay

We have previously studied the structure of colloidal aggregates in great detail using an aggregation model developed in earlier parts of this project. The objective of our most current work is to extend our study to the density profiles of aggregated networks near a hard wall where the hard wall is a simplification of the surface of a large particle.

Increasingly, colloidal processing of ceramic materials requires the mixing of two or more different kinds of particles at the colloidal scale for purposes such as reaction sintering, sintering aids, and the fabrication of composite materials. Often, the mixing involves particles of very different sizes, e.g., large particles of material *A* mixed with much smaller particles of material *B*. The density variation in the interfacial region near the surface of a large particle is important in controlling sintering as well as in determining the final properties of the specimen. Since small particles often form aggregates, in this work we focus on the density profiles of aggregated

networks formed by the small particles near the surface of a large particle. The interaction between the large particles and the small particles is assumed to be nonattractive in this work.

The density profiles of aggregated networks of the small particles near a hard wall are simulated using the aggregation model previously developed. The density variations near the hard wall will be related to the structure of the network. A scaling theory was also developed to explain the density variations near the wall.

We found that similar to those of polymeric networks near a hard wall, the density profiles of colloidal aggregated networks near a hard wall can be described by the form that we derived previously for polymer networks:

$$\phi(z) = \phi_0[1 - e^{-(z/\xi)^m}], \tag{1}$$

where z is the distance away from the wall, ϕ_0 the bulk density of the aggregated network, and ξ and m are the parameters that characterize the structure of the network; m turns out to be the fractal dimension, D, of the aggregates that pack to form the network and ξ the size of the blobs, i.e., the structural units of the network.

The width of the depletion layer is on the order of the average blob size ξ. A scaling analysis was developed that showed that ξ decreases with an increasing bulk density ϕ_0 as

$$\xi \sim \phi_0^{-1/(d-D)}, \tag{2}$$

where d is the Euclidean dimension, D the fractal dimension of the network. Eqn. (2) is in good agreement with the results of our simulations. A manuscript is being written to be submitted to *Physical Review A*.

1.2.6 Synthesis of Lead-Zirconium-Titanate ($Pb(Zr_{0.52}Ti_{0.48})O_3$) (PZT) Powders for Low-Temperature Sintering

Investigators: F. Dogan and I. A. Aksay

Low-temperature sintering of ceramic materials is often desirable to attain fine grain microstructures for improved physical properties in the final material. In the case of lead zirconium titanate ($Pb(Zr_{0.52}Ti_{0.48})O_3$) (PZT), low temperature sintering is especially important since we are interested in determining the effect of grain size on pieozoelectric properties. Further, if grain size can be kept to < 0.3 μm, it is possible to produce fully dense and optically transparent PZT for use in nonlinear optical applications. Thus, our goal has been: (i) to synthesize nanometer sized PZT powder that would be suitable for low-temperature sintering and (ii) to investigate the effect of grain size on piezoelectrical and electrooptical properties in dense monoliths.

Powders were prepared by three different techniques: (i) aerosol spray pyrolysis (ASP), (ii) spray pyrolysis followed by flashing (explosive oxidation of mixtures of sucrose and metal nitrate powders), and (iii) coprecipitation combined with freeze drying of metal solutions. Powders of low yield and poor crystallinity were obtained by aerosol spray pyrolysis. Powders prepared by spray drying and pyrolysis were found to contain hard agglomerates that were difficult to break into smaller particles. Powders made by freeze drying contained soft

agglomerates, allowing compacts with a small pore size and narrow pore-size distribution to be made. Because soft agglomerates are more amenable to further processing, the freeze drying process became the subject of this work.

Samples sintered from freeze-dried powders achieved densities as high as 98.5% of the theoretical density. The average grain size was about 1 μm. The sintering temperature of 800°C represented a significant reduction from the liquid phase sintering that has been done at 1200°C. The lowest eutectic in the phase diagram of PZT lies at 860°C, indicating that densification in our samples is not through liquid phase sintering. We propose that densification is improved by two factors: (i) enhanced surface diffusion by excess PbO and (ii) the narrow pore size distribution in the powder compacts prior to sintering.

The samples sintered at low temperatures exhibited very good piezoelectric response. Experiments are now in progress to determine the effects of the small grain size and the absence of dopants upon these properties. Nb-doped powders will be synthesized and their sintering behavior studied. The piezoelectric properties of the doped samples will be compared with undoped and low-temperature sintered samples.

1.2.7 Perovskite Seeding of Sol-Gel Lead-Zirconate-Titanate ($Pb(Zr_{0.52}Ti_{0.48})O_3$) Thin Films for Low-Temperature (<500°C) Perovskite Formation

Investigators: W. D. Clifton and I. A. Aksay

This research has led to the development of a novel method for depositing ferroelectric thin films in which crystallization can be controlled. The method provides an advantage over existing methods due to the low temperature of deposition required to produce dense single phase thin films. Thin (< 1 μm) films of ferroelectric lead-zirconate-titanate (PZT) are of interest for numerous microelectronic applications including non-volatile memories, piezoelectric microsensors and actuators, optical memories, and dielectric layers. Many methods exist for depositing PZT films, but they all fail to meet the low temperature (<500°C) processing requirement for direct-gap semiconducting substrates (e.g., GaAs). Thus the goal of our research has been to reduce this processing temperature by the method summarized below.

Current methods of producing $Pb(Zr_{0.52}Ti_{0.48})O_3$ ferroelectric thin films exhibit very sluggish crystallization. We have identified the causes of this sluggish crystallization. At temperatures around 450-475°C, the films begin to crystallize, but initially an undesirable pyrochlore phase crystallizes. The pyrochlore phase does not exhibit any of the dielectric, ferroelectric, or electrooptic properties which the desirable perovskite phase does. Crystallization of the perovskite phase occurs very slowly and requires temperatures above 650°C. The perovskite nucleates at 525°C, but the density of nucleation sites is very low. To convert the film to full perovskite, the perovskite grains grow into the pyrochlore matrix; long processing times are required to complete this process. Thus, two problems have been identified which inhibit low temperature crystallization: (i) the perovskite does not even nucleate until 525°C and (ii) the density of perovskite nucleation sites is too low.

The evolution of lead from the pyrochlore matrix is an additional hindrance to perovskite crystallization. Atomic force microscopy (AFM) and TEM studies of these films indicate that the pyrochlore matrix is very fine grained (< 20 nm) and the grains thus have a high surface area in contact with the furnace atmosphere. This causes significant losses of lead from the pyrochlore matrix. The perovskite does not have as high a surface area and does not lose lead as readily. TEM analysis of these films using energy dispersive analysis (EDS) has shown significant

variations in the lead content between the pyrochlore and perovskite regions. We have observed that as the perovskite grains grow into the pyrochlore matrix, the pyrochlore phase loses lead to the perovskite phase which remains stoichiometry. The loss of lead to the atmosphere and from the pyrochlore to the perovskite phase decreases the rate of perovskite crystallization by increasing the diffusion distance of the remaining lead ions to the perovskite phase. Ultimately, insufficient lead may be present in the remaining pyrochlore phase and further conversion to perovskite will be impossible.

Our research first investigated methods of reducing the crystallization temperature by studying different methods for producing the polymeric film precursor solution and the effect of the resulting precursor on the crystallization behavior of the film. Different precursors were synthesized by changing the substituent alkyl groups, varying the conditions of hydrolysis, and catalyzing polymerization with different acids and bases. No significant improvements in the crystallization behavior were observed with any of these variations; also, all samples formed the pyrochlore phase during heating.

We then turned to a novel approach of placing crystalline perovskite PZT particles (produced by the methods described in Section 1.2.3) within the precursor gel. Subsequent characterization of these gels indicated that crystallization occurred over a much narrower temperature range and that the perovskite phase could be fully formed at significantly lower temperatures. Differential thermal analysis (DTA) measurements revealed that crystallization in these seeded gels was complete at temperatures below 530°C.

Building on these results, we refined our process to use nanometer-sized PZT particles as seeds in films as thin as 200 nm. The particles were first produced by heating freeze-dried, co-precipitated PZT precursor particles to 700°C to ensure complete perovskite crystallization. A monolayer coating of these PZT particles was then deposited on the substrate surface. The film precursor gel was spin-coated over the surface resulting in an amorphous PZT film containing PZT seeds.

Characterization of these seeded films revealed dramatic improvements in the crystallization behavior. When heated to temperatures of 460°C or greater, the films crystallized to perovskite PZT. No evidence of pyrochlore formation was observed. By microscopic observations, the density of heterogeneous nucleation sites in the seeded films was found to be over three orders of magnitude greater than that observed for the unseeded films. This dramatically lowered the necessary diffusion distances, allowing the more stable perovskite phase to form readily throughout the film. Measurements of the ferroelectric and dielectric properties of these lower temperature films indicate that they have equivalent properties to unseeded films heated to 650-700°C (Fig. 7): seeded PZT films heated to 500°C had a dielectric constant of 700 with a remnant polarization of 11 $\mu C/cm^2$. An invention disclosure has been filed on this process through the Washington Technology Center, Seattle, Washington.

1.2.8 High-Density Barium Titanate Ceramics

Investigators: K. Shinozaki, W. C. Hicks, and I. A. Aksay

In order to study the grain size effects on the properties of dense $BaTiO_3$ monoliths and thin films, it is first necessary to develop methods to process them with nanometer- to micrometer-sized grains. Processing of nanosized grain structures is also useful for attaining transparency in polycrystalline ceramics. Previous studies have shown that principal factors affecting the structural evolution during densification are pore size distribution, total pore volume, grain size

distribution, and the grain growth mechanism.[6] As summarized below, our focus in the processing of $BaTiO_3$ has been to investigate the role of these parameters on the densification of monoliths and thin films in order to study the effect of grain size on ferroelectric properties. A longer range goal is also to produce transparent polycrystalline barium titanate and thus eliminate the need to use single crystals for nonlinear electrooptical applications.

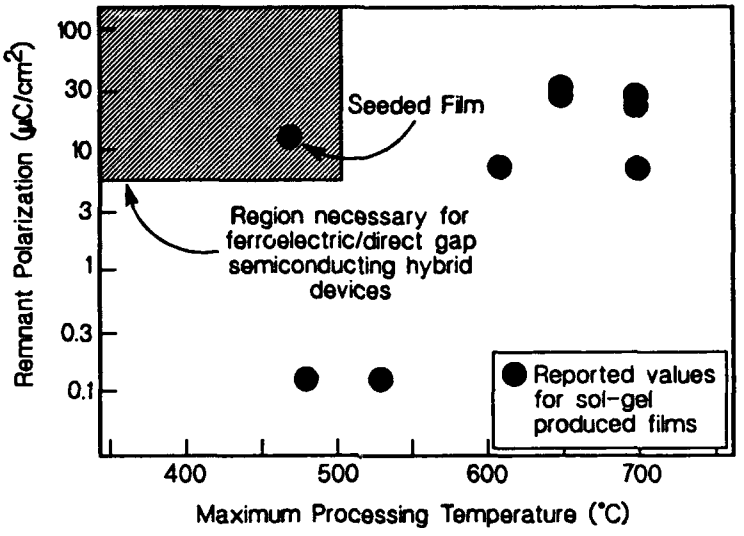

Figure 7: Remnant polarization versus heat treatment temperature for PZT thin films produced by the seeding method developed in our laboratory as compared to the results from other studies.

Our experimental approach consisted of four steps to produce dense, transparent barium titanate: (i) the hydrothermal reaction of titanium oxide in barium hydroxide solution; (ii) novel colloidal processes to produce well-dispersed slurries followed by consolidation by pressure filtration; (iii) infiltrating barium titanate precursors and desired additives into an unsintered green body, both to increase the green density and to control the pore-size distribution; and (iv) low-temperature sintering of consolidated powder compacts. Powder suspensions were filtered under pressure to form uniformly consolidated compacts. The compacts were at 58% of theoretical density and contained 27 vol% very fine pores (median pore size: ~16 nm) having a narrow pore-size distribution. The volume of the polymeric surfactant which was used to stabilize the suspensions accounted for about 15 vol% in the compact and this led to increased porosity during sintering. Through an infiltration process of these compacts, we have produced translucent samples, but true transparency has yet to be achieved.

2. Ceramic Matrix Composites: Processing and Properties

This portion of our project continues work on ceramic matrix composites that first began in our group in 1983. The key emphasis is on the application of fundamental concepts generated in our previous projects to produce novel composites that can be utilized in engineering applications. Since the initial studies on boron carbide/aluminum composites, composite material research has expanded to include ceramic/polymer laminates and nanocomposites produced by a novel reaction sintering method. The results of our work on ceramic/polymer composites appeared in the final report for our preceding "Microdesigning of Lightweight/High-strength Ceramic Materials" project (the final phase of which overlapped the first few months of the current project) and that work will be continued in subsequent portions of this current project. Research on boron

carbide/aluminum composites is continuing with specific emphasis on the strengthening mechanisms.

2.1 Synthesis of SiC/Mullite/Alumina Nanocomposites by Reaction Sintering

Investigators: Y. Sakka, D. D. Bidinger, and I. A. Aksay

Nanocomposite materials that are composed of nanometer-size second-phase particles dispersed in a ceramic matrix are expected to have excellent mechanical and electrical properties. Possible synthesis methods for nanocomposites include: (i) synthesis from mixtures or composites of nano-sized fine particles, (ii) synthesis from mechanically alloyed powders, and (iii) synthesis by reaction sintering. The first method is limited because of the difficulty in producing the dispersed nano-sized particles. Mechanical alloying can be inconsistent in producing materials. In this work, we demonstrate a new method for synthesizing nanometer-sized SiC particles dispersed in a mullite/alumina matrix using reaction sintering.

After the green compacts of mixtures of alumina and SiC powders were prepared by colloidal processing, the following two steps were performed: (i) the surface of the SiC particles was oxidized to produce silicon dioxide and to reduce the size of the remaining SiC down to the nanometer scale; (ii) this was followed by reaction sintering in which a matrix of mullite was produced by reacting the silicon dioxide with alumina, leaving the SiC particles suspended in the matrix material.

Alumina and SiC powders were dispersed using PMAA in aqueous solution at high pH in order to obtain high-density green compacts. These suspensions were consolidated by filtration. The densities of the green bodies were 62 to 64% of theoretical density. Reaction sintering was carried out at temperatures ranging from 1550° to 1750°C for 2 or 5 h in an argon atmosphere. During sintering the cristobalite phase disappeared and mullite was produced. The quantity of mullite produced depended on the extent of oxidation in the SiC. Moreover, the oxidation treatment was effective in forming high-density sintered bodies. SEM and TEM experiments are now planned to determine the degree of SiC dispersion and the structures of the interfaces.

2.2 Mullite-$MoSi_2$ Composites

Investigators: R. Brynsvold, J. E. Webb, D. L. Milius, and I. A. Aksay

Currently, only metals and metal matrix composites are used for high-temperature (>1000°C) structural applications in the aerospace industry due to their high strength and stiffness. However, these materials are costly and heavy. In this project, we were interested in fabricating a ceramic composite with high strength, low density, and good oxidation resistance. We have investigated the use of mullite ($3Al_2O_3 \cdot 2SiO_2$) as a matrix material, reinforced by inclusions of $MoSi_2$, a material which has long been used for heating elements in air furnaces. $MoSi_2$ forms a protective amorphous silica layer on its surface when exposed to oxygen at high temperatures preventing further oxidation. In addition, $MoSi_2$ undergoes a brittle to plastic transition at around 900-1000°C giving it the ability to act as the ductile phase in the composite.

So far, no one appears to have investigated the use of mullite-$MoSi_2$ composites in high-temperature applications. However, previous work on oxidation kinetics of mullite demonstrated that it is a suitable matrix for containing an oxidizable siliceous phase. We have determined that mullite and $MoSi_2$ are phase compatible and may be processed to 93% theoretical density (containing 20 vol% $MoSi_2$) with hot pressing. The toughness of hot pressed composites increased to 3 to 4 $MPa \cdot m^{1/2}$ (K_{Ic}), with strengths ranging from 230 MPa (15 vol% $MoSi_2$) to 420

MPa (20 vol% $MoSi_2$). The material was found to be self-healing due to the protective silica layer on the $MoSi_2$ particles in the matrix.

We have fabricated samples using hot pressing but have also tried alternate pressureless sintering methods. In particular, we coated $MoSi_2$ particles with silica, then dispersed those particles in a mullite-forming gel. The procedure used was developed during the last stage of our "Microdesigning of Lightweight/High Strength Ceramic Materials" project using silicon carbide as the reinforcing phase in mullite.

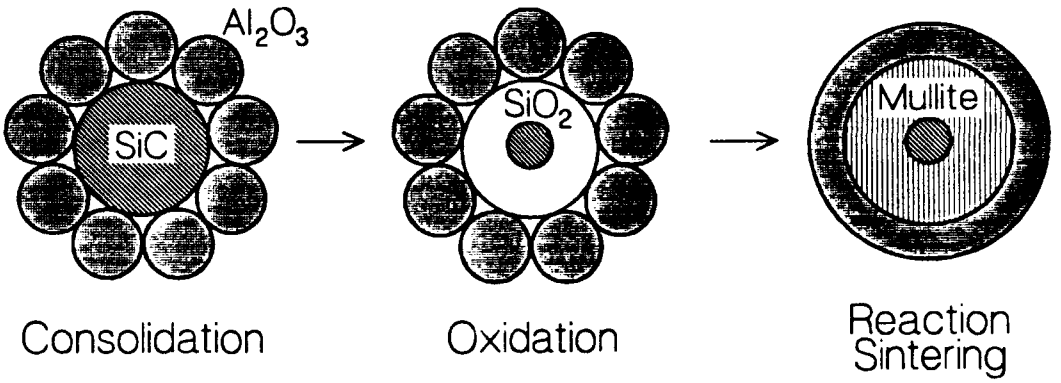

Figure 8: Schematic illustration of the reaction sintering of coated particles to produce nanocomposites.

2.3 Processing of SiC/Al

Investigators: Y. L. Zhang, K. Janghorban, M. Yasrebi, D. L. Milius, and I. A. Aksay

Silicon carbide possesses low density, good strength retention at high temperatures, and excellent resistance to oxidation. In fiber, whisker, or particulate forms it has been widely used for making metal matrix composites. However, silicon carbide readily reacts with liquid aluminum to form the mechanically poor product Al_4C_3, making the fabrication of a SiC/Al ceramic matrix composite with high specific strength extremely difficult. Our goal in this project is to develop a processing method to produce Al_4C_3-free SiC/Al composites with excellent mechanical properties.

In order to eliminate or minimize the formation of Al_4C_3, two approaches have been taken: (i) oxidation of the SiC surface and (ii) coating the SiC surface with silicon. These approaches have not completely solved the problem since any exposed SiC reacts with the aluminum to form Al_4C_3. Our goal in this project was to use pressureless sintering and vacuum filtration to make samples of Al_4C_3-free SiC/Al suitable for mechanical property testing. Large SiC/Al ceramic matrix composite samples had not been made by the start of this project.

SiC powder and sintered monoliths were decarbonized to remove free carbon and thereby suppress formation of Al_4C_3. We subsequently found that the monoliths could not be infiltrated with either aluminum or aluminum-silicon melts following decarbonization. In an effort to improve wetting, titanium was added to the SiC powder, which also aided in the removal of free carbon. After sintering, the monoliths could be infiltrated with aluminum-silicon melts. Infiltration appeared to be nearly complete and analysis by x-ray diffraction indicated that no Al_4C_3 formed in samples infiltrated with aluminum containing 20% Si. There were defects in the samples which may be have been caused by depletion. The strength of our composites were measured using three-point flexural strength testing. The average strength was 455 MPa.

Our subsequent work on the SiC/Al composite system will include TEM analysis of the interfaces. We hope to determine the causes of defect formation and thereby eliminate them from the sintered monoliths. We need to understand wetting to determine if mechanical properties can be improved by doping the aluminum-silicon alloys with trace elements or through heat treatment.

2.4 The Effect of the Metallic Phase and Microstructure on the Strengthening Behavior of B_4C-Al Cermets

Investigators: G. H. Kim, M. Sarikaya, and I. A. Aksay

In our previous studies, we have successfully developed processing techniques to fabricate monolithic B_4C-Al ceramic-metal composites (density 2.65 g/cc) with fracture toughness and fracture strength of 10 MPa·m^{½} (3-point SENB test) and 670 MPa (4-point bending), respectively. These values are much higher than what can be expected from the existing theories such as rule of mixture on the strength of the composites. Further increases in the fracture strength up to 950 MPa and toughness up to 16 MPa·m^{½} were observed in the laminated B_4C-Al composites (Fig. 8). There is currently no satisfactory explanation of the strengthening behavior observed for cermets such as WC-Co, SiC-Al, and B_4C-Al. The goal of this part of our project is to determine the respective roles of the metal phase and the microstructure of the composite in the observed increase in physical properties.

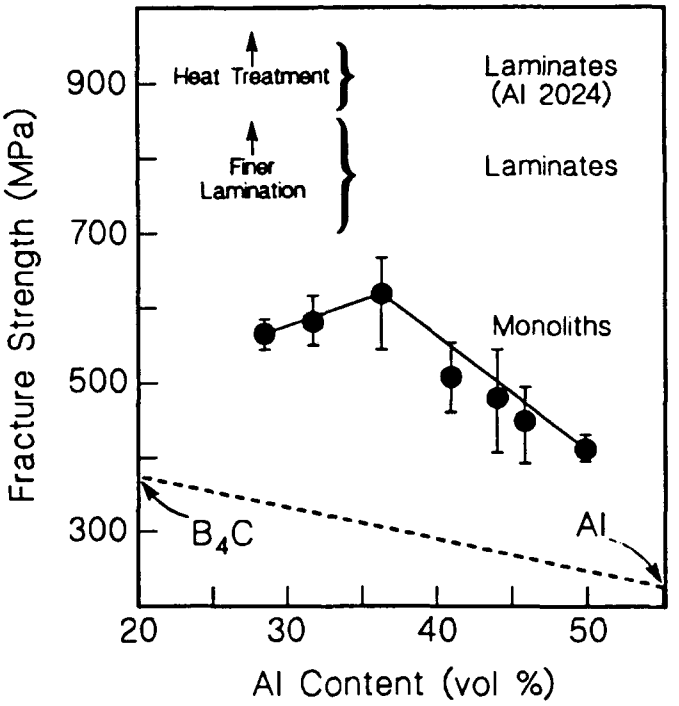

Figure 9: The observed strength of B_4C-Al cermets as a function of Al content. This can be compared to the results expected from using the rule of mixture to model strength.

The role of the microstructure was studied for B_4C-Al composites by varying the grain size in the ceramic phase, the volume fraction of aluminum, and the types of aluminum alloys used as the ductile phase. Microlaminates of B_4C-Al composites with graded (thick/thin) microstructures were made by tape casting individual layers, then pressing together and infiltrating several layers to form the structure. The strength dependence on the scale of lamination was examined using

two lamination schemes: 600 μm/100 μm and 75 μm/13 μm laminates; the thicker layers contained 32 vol% and the thinner layers 45 vol% aluminum respectively (resulting in an average aluminum content of 34 vol%). The strength increase in the finer laminates was not as high as expected, with 860 MPa the maximum obtained for 75 μm/13 μm laminates made using All 1100 alloy. Compared to monolithic cermets of similar composition, we observed a 30% increase in strength and a 10% increase in toughness. Laminated cermets also exhibited higher resistance to crack initiation.

When laminated B_4C-Al composites made using Al 2024 alloy were aged, the maximum strength observed was 935 MPa. Microstructural changes in the aluminum phase were observed due to the high thermal stress in the ductile phase.

Base on predictions from the rule-of-mixtures, we propose two possible mechanisms for the increased strength in laminated B_4C-Al cermets: The first involves the contribution from the monolithic microstructure of the ceramic phase, the second mechanism involves the lamination itself. In the case of the lamination, we considered the variation in the bridging zone size which leads to the variation in the strength due to a steep R-curve. The R-curve strengthening may provide a better explanation for the lamination effect as the thickness of the lamination ranges from 80 to 600 μm.

Direct correlation between the magnitude of thermal stresses in the cermet and its strength was determined for three cermet systems of different characteristics. The technique of convergent beam electron diffraction, CBED, was used to measure local strains on the order of 10^{-4} from regions as small as 30 nm. Standard metal phases were used for accurate determination of thermal strain in the metals, and results showed that approximately 3×10^{-3} strain existed in the metal phases, equivalent to residual tensile thermal stresses of about 3 times the yield strength in the aluminum region of the B_4C-Al cermet. Although it was difficult to get accurate measurements of the stresses in the cobalt region of WC-Co cermets (due to the metastability of the cubic Co phase), approximately 1 GPa of thermal stress was measured in the isolated cobalt regions of the cermet. In SiC-Al cermets, the thermal stress in the aluminum regions were much smaller than in the B_4C-Al cermet, possibly due to the lower contiguity in the ceramic phase.

Similar to the strength of laminated and monolithic B_4C-Al cermets, the toughness of monolithic boron carbide-aluminum cermets originate from bridging zone formation by aluminum ligaments behind the crack tip. Constrained metal ligaments exhibit 2 to 6 times higher yield strength than that of bulk aluminum and this becomes the main toughening mechanism. For laminated microstructures, two other factors contribute to the ability to stop crack propagation or increase the toughness: the repeat distance of the ductile layer and the ductility of the same. As the scale of lamination becomes finer, the repeat distance decreases and increasing constraints are observed on the ductile phase; this ultimately results in a toughness which is no longer affected by the laminate thickness. The ductility of the thin layer was evaluated using microhardness measurements and by observing the behavior of indentation cracks as a function of the layer thicknesses. It was observed that the ductility decreased with decreasing layer thicknesses.

The future design of high performance ceramic-metal composites can benefit by following the guidelines established in this study. First, an interconnecting microstructure is the most important parameter since it provides both elastic and plastic constraints necessary for simultaneous strengthening and toughening. Second, liquid phase processing (i.e., the metal or ductile phase) is preferable since the interface needs to be strong enough to accommodate interfacial shear stress developed by thermal expansion mismatch. Both interpenetrating microstructure and strong

interfaces will retain the hydrostatic tensile stress in metal phase which provides compressive stress in the ceramic phase and thus strengthens the ceramic phase. In order to exploit the thermal strain in the metal phase, a ductile phase with high elastic modulus is preferable in order to establish the elastic constraint mechanism for strengthening. On the other hand, a ductile phase with a high yield strength is recommended for maximum plasticity, required for effective toughening via the formation of a bridging zone.

Further enhancement of mechanical properties can be made by employing macroscopic modification of the microstructure, such as increasing the scale of lamination to the millimeter scale where the size effect is insignificant. Enhanced strength by lamination is possible by designing composites with very short bridging zone size and with large differences between the initial and steady state values of fracture toughness. Toughness enhancement, on the other hand, can be done by using highly ductile layers with small repeat distances.

2.5 Processing and Structure-Property Relationships of Boron Carbide/Polymer Composites

Investigators: S. Khanuja, G. H. Kim, D. R. Treadwell, M. Yasrebi, and I. A. Aksay

Laminated boron carbide/polymer composites were developed in order to enhance the damage tolerance of B_4C ceramics. The composites were fabricated by infiltrating polymers in partially sintered (66 vol% dense) B_4C tapes suing solution infiltration, melt infiltration, and *in situ* polymerization techniques. It was determined that melt infiltration was the best technique for preparing laminated ceramic-polymer composites (cerpolys) with semicrystalline polymers, such as polyethylene (PE) and polypropylene (PP). The work of fracture (WOF) of laminated B_4C/PP and B_4C/PE composites was measured as 870 J/m^2 and 580 J/m^2, respectively. These values are 30 to 40 times higher than the WOF of fully dense B_4C preforms. *In situ* fracture analysis showed that polymer bridging is the most dominant toughening mechanism of these composites. The effect of interface and size of the microstructure on the extent of polymer bridging was also investigated. Interface analysis revealed that an optimum amount of debonding is required to maximize the WOF of these composites. The study of size effect was very complex because a change in the scale of microstructure of the laminated composites has been shown to affect the microstructure of the polymer significantly.

3. References

1. J. Liu, research report, University of Washington (1991).
2. J. Liu, W. Y. Shih, M. Sarikaya, and I. A. Aksay, "Selfdivision and Monodispersity of Colloidal Gold", to be submitted to *Science*, 1992.
3. J. Liu, W. Y. Shih, M. Sarikaya, and I. A. Aksay, "Fractal Colloidal Aggregates with Finite Interparticle Interaction: Energy Dependence of the Fractal Dimension", *Phy. Rev. A*, **41**, 3206 (1990).
4. M. Dommadieu, *Materials Science and Engr.*, **B3** 185-195 (1989).
5. A. Chemseddine, R. Morineau, and J. Livage, *Solid State Ionics*, **9**, 357-362 (1983).
6. A. I. Kingon and J. B. Clark "Sintering of PZT Ceramics: I, Atmosphere Control, *J. Amer. Ceram. Soc.*, **66**, 252-256 (1983).
7. W. Hertl, "Kinetics of Barium Titanate Synthesis," *J. Am. Ceram. Soc.*, **71** [10] 879-83 (1988).
8. C. Han, I. A. Aksay, and O. J. Whittemore, "Characterization of Microstructural Evolution by Mercury Porosimetry," ***Advances in Materials Characterization II***, edited by R. C. Snyder, R. A. Condrate, Sr., and P. F. Johnson (Plenum, New York, 1985) pp. 167-78.
9. K. W. Kirby and B. A Wechsler, "Phase Relations in the Barium Titanate-Titanium Oxide System," *J. Am. Ceram. Soc.*, **74** [8] 1841-47 (1991).
10. G. Pfaff, F. Schmidt, W. Ludwig, and A. Feltz, "$M^{II}TiO(C_2O_4)_2 \cdot 4H_20$ (M^{II} = Mg, Ca, Sr, or Ba) As Precursors in the Formation of $M^{II}TiO_3$ Powders," *J. Thermal Anal.*, **33** 771-779 (1988).
11. A. N. Christensen and S. E. Rasmussen, "Hydrothermal Preparation of Compounds of the Type ABO_3 and AB_2O_4," *Acta Chem. Scand.*, **17**, 845 (1963).
12. S. Somiya, "Hydrothermal Preparation of Fine Powders," in ***Advanced Ceramics III***, edited by S.Somiya, Elsevier Science Publishers LTD, 247-243, (1990).
13. E. Lilley and R. R. Wusirika, "Method for the Production of Mono-Size Powders of Barium Titanate", U.S. Patent Number: 4,764,493, Aug. 16,1988.
14. K. Abe and S. Matsumoto, "Hydrothermal Processing of Functional Ceramic Powders", in ***Ceramic Powder Science IV***, The American Ceramic Society, 15-25.
15. D. M. Pepper, J. Feinberg, and N. V. Kukhtarev, "The Photorefractive Effect" *Scientific American*, 62-74, October 1990
16. N. A. Ovremenko, L. I. Shvets, F. D. Ovcherenko, and B. Y. Kornilovic, "Kinetics of Hydrothermal Synthesis of Barium Metatitanate", *Inorganic Materials*, 1560-1562, (1980)
17. K. Oseeo-Asare, F. J. Arriagada, and J. H. Adair, "Solubility Relationship in the Coprecipitation Synthesis of Barium Titanate: Heterogeneous Equilibria in the Ba-Ti-C_2O4-H_2O-System", ***Ceramic Powder Science II***, edited by: G. L. Messing, E. R. Fuller Jr, H. Hausner, The American Ceramic Society Inc., Westerville, OH 1988
18. M. Yoshimura, S. E. Yoo, M. Hayashi, and N. Ishizawa, "Preparation of $BaTiO_3$ Thin Film by Hydrothermal Electrochemical Method", *Jap. J. Appl. Phys.*, **28**, 2007-2009 (1989)
19. D. Hennigs, G. Rosenstein, and H. Schreinemacher, "Hydrothermal Preparation of Barium Titanate from Barium-Titanium Acetate Gel Precursors", *J. Europ. Ceram. Soc.* **8**, 107-115, (1991)

20. E. Tani, M. Yoshimura, and S. Somiya, "Formation of Ultrafine Tetragonal ZrO_2 Powder under Hydrothermal Conditions", *J. Am. Ceram. Soc.*, **66**, 11-14, (1983)
21. D. J. Watson, C. A. Randall, R. E. Newnham, and J. H. Adair "Hydrothermal Formation Diagram in the Lead Titanate System", in ***Ceramic Powder Science II***, 154-162, (1988)
22. R. P. Denkewicz, Jr., K. S. Ten Huisen, and J. H. Adair, "Hydrothermal Crystallization Kinetics of m-ZrO_2 and t-ZrO_2", *J. Mater. Res.*, **5**, 2698-2705, (1990)
23. R. Egerton, ***Electron Energy Loss Spectroscopy in the EM***, Plenum, New York (1986).
24. D. E. Sayers, E. A. Stern, and F. W. Lytle, *Phys. Rev. Lett.*, **27**, 1204-1207 (1971).
25. M. Kundman, ***EL/P Software Instruction Manual***, GATAN, Inc. (1992).
26. R. D. Leapman and V. E. Cosslett, *J. Phys. D (J. Appl. Phys.)*, **9**, 129 (1976).
27. E. A. Stern, *Optic*, **61**, 45 (1982).
28. M. Qian and M. Sarikaya, unpublished research (1992).
29. M. Qian and M. Sarikaya, XAFS Software (UWXAFS 2.0), University of Washington.
30. J. J. Rehr, *J. Am. Chem. Soc.*, **113**, 5135 (1991).
31. A. Ziabicki, ***Fundamentals of Fibre Formation***, John Wiley and Sons, London, (1976).
32. L. E. Seufert, "Alumina Fiber," U.S. Patent #3,808,015 (April 30, 1974).
33. H. G. Sowman, "Aluminum Borate and Aluminum Borosilicate Articles," U.S. Patent #3,795,524 (March 5, 1974).
34. J. C. Romine, "Aluminum Oxide Fibers," ***High Technology Fibers -- Part B; Handbook of Fiber Science and Technology: Volume III***, Eds. M. Lewin and J. Preston, Marcel Dekker, Inc., New York, 151-174, (1989).
35. J. C. Romine, "New High-Temperature Ceramic Fiber," *Ceramic Engineering and Science Proceedings*, **8** [7-8], American Ceramic Society, Columbus OH, 755-765 (1987).
36. S. Yajima, J. Hayashi, M. Omori, and K. Okamura, "Development of a Silicon Carbide Fibre with High Tensile Strength," *Nature*, **261**, 683-685 (July 24, 1976).
37. S. Yajima, K. Okamura, J. Hayashi, and M. Omori, "Synthesis of Continuous SiC Fibers with High Tensile Strength," *J. Am. Ceram. Soc.*, **59** [7-8], 324-327, (1976).
38. V. M. McNamara, "A Wet Chemical Method for the Preparation of Oxide Mixtures Applicable to Electronic Ceramics," *J. Can. Ceram. Soc.*, **34**, 103-120 (1965).
39. G. H. Haertling and C. E. Land, "Hot-pressed (Pb, La) (Zr, Ti)O_3 Ferroelectric Ceramics for Electrooptic Applications," *J. Am. Ceram. Soc.*, **54**, 1-11 (1971).
40. R. B. Atkin and R. M. Fulrath, "Point Defects and Sintering of Lead Zirconate-Titanate," *J. Am. Ceram. Soc.*, **54**, 265-270 (1971).
41. A. I. Kingon and J. B. Clark, "Sintering of PZT Ceramics: II, Effect of PbO Content on Densification Kinetics," *J. Am. Ceram. Soc.*, **66**, 256-260 (1983).
42. D. E. Wittmer and R. C. Buchanan, "Low-Temperature Densification of Lead Zirconate-Titanate with Vanadium Pentoxide Additive," *J. Am. Ceram. Soc.*, **64**, 485- 490 (1981).
43. G. Tomandl, A. Stiegelschmitt, and R. Boehner, "Lowering the Sintering Temperature of PZT-Ceramics by Sol-Gel Processing," *Sci. Ceram.*, **14**, 305-308 (1988).
44. G. W. Scherer, "Viscous Sintering of Particle-Filled Composites," *Bull. Am. Ceram. Soc.*, **70** [6] 1059-1063 (1991).
45. M. D. Sacks, W. Bozkurt, and G. W. Scheiffele, "Fabrication of Mullite and Mullite-Based Composites by Transient Viscous Sintering of Composite Powders," *J. Am. Ceram. Soc.*, **74** [10] 2428-2437 (1991).

46. M. P. Borom, M. K. Brun, and L. E. Szala, "Kinetics of Oxidation of Carbide and Silicide Dispersed Phases in Oxide Matrices," *Adv. Ceram. Mat.*, **3** [5] 491-97 (1988).
47. T. Iseki, et al., "Interfacial Reactions Between SiC and Al During Joining," *J. Mat. Sci.*, **19** (1984).
48. D. J. Lloyd, et al., "Microstructural Aspects of Aluminum-Silicon Carbide Particulate Composites Produced by a Casting Method," *Mat. Sci. Eng.*, A 107 (1989).
49. D. L. Milius, "The Sintering of Silicon Carbide with Liquid Aluminum," M.Sc. Thesis, University of Washington, 1986.
50. D. H. Stutz, S. Prochaszka, and J. Lorenz, "Sintering and Microstructure Formation of b-Silicon Carbide," ***Ceramic Transactions, Silicon Carbide '87*, Vol. 2.**
51. M. Robert Baungartner, et al., "Pressureless Sintering and Properties of Plasma Synthesized SiC Powder," ***Ceramic Transactions, Silicon Carbide, '87*, Vol. 2.**
52. S. Shinozaki, et al., "Analytical Electron Microscopy on the Effects of Sintering Aids in Pressureless Sintered SiC Materials," ***Advanced Ceramics***, edited by Shigeyuki Somiya, 1986.
53. M. Yasrebi, G. H. Kim, K. E. Gunnison, D. L. Milius, M. Sarikaya, and I. A. Aksay, "Biomimetic Processing of Ceramics and Ceramic-Metal Composites", *Mat. Res. Soc. Symp. Proc., Vol.* **180**, 1990.
54. M. Yasrebi, G. H. Kim, D. L. Milius, M. Sarikaya, and I. A. Aksay, "Processing and Characterization of B_4C-AL Laminated Cermets", *Proc. XXIIth International Congress for Electron Microscopy* (San Francisco Press, San Francisco, 1990) pp. 1022-23.
55. A. J. Pyzik and I. A. Aksay, "Microdesigning of B_4C-Al cermets," in ***Processing of Ceramic and Metal Matrix Composites***, edited by H. Mostaghaci (Pergamon Press, New York, 1989), pp. 269-80.
56. A. J. Pyzik, I. A. Aksay, and M. Sarikaya, "Microdesigning of Ceramic-Metal composites," in ***Ceramic Microstructures '86***, edited by J. A. Pask and A. G. Evans (Plenum, New York, 1987), pp. 45-54
57. D. C. Halverson, A. J. Pyzik, I. A. Aksay, and W. E. Snowden, "Processing of Boron Carbide-Aluminum Composites," *J. Am. Ceram. Soc.*, **72**[5] 775-80(1989)
58. M. Yasrebi, G. H. Kim, D. L. Milius, M. Sarikaya, and I. A. Aksay, "Biomimetic Processing of Ceramics and Ceramic-Metal Composites," in ***Better Ceramics through Chemistry IV*, *MRS Symp. Proc., Vol* 180**, edited by C. J. Brinker, D. E. Clark, D. R. Ulrich, and B. J. J. Zelinksi (Materials Research Society, Pittsburgh, Pennsylvania, 1990), pp. 625-35

4. Personnel

Senior Research Personnel:

I. A. Aksay	Y. Sakka
D. M. Dabbs	M. Sarikaya
F. Dogan	W.-H. Shih
B. Flinn	W. Y. Shih
K. Janghorban	K. Shinozaki
J. Liu	Y. B. Son
M. Qian	D. R. Treadwell

M. Yasrebi

Junior Research Personnel:

R. Brynsvold	G. Magendanz
W. M. Carty	D. L. Milius
W. D. Clifton	K. Sastry
S. Khanuja	J. E. Webb
G. H. Kim	T. Yoshimori

Y. L. Zhang

Undergraduate Research Personnel:

D. B. Bidinger	L. C. Thompson
D. Ellerby	I. G. Vahora
G. Mehler	A. M. Waymire

J. R. Woodard

5. Manuscripts

1991

1. I. A. Aksay, "Molecular and Colloidal Engineering of Ceramics," in ***Ceramics Today–Tomorrow's Ceramics: Proc. 7th CIMTEC World Ceramics Congress and Satellite Symposia,*** edited by P. Vincenzini (Elsevier, Amsterdam, 1991), pp. 49-60.
2. I. A. Aksay, "Molecular and Colloidal Engineering of Ceramics," *Ceramics International*, **17**, pp. 267-74 (1991).
3. W. Y. Shih, J. Liu, W.-H. Shih, and I. A. Aksay, "Aggregation of Colloidal Particles with a Finite Interparticle Attraction Energy," *J. Stat. Phys.*, **62** [5/6] 961-84 (1991).
4. I. A. Aksay, D. M. Dabbs, and M. Sarikaya, "Mullite for Structural, Electronic, and Optical Applications," *J. Am. Ceram. Soc.*, **74** [10] 2343-58 (1991).
5. I. A. Aksay and M. Sarikaya, "Bioinpsired Processing of Composite Materials," in ***Ceramics: Toward the 21st Century, Centennial International Symposium***, edited by N. Soga and A. Kato (Ceramic Society of Japan, Tokyo, 1991), pp. 136-49.
6. S. Sundaresan and I. A. Aksay, "Mullitization of Diphasic Aluminosilicate Gels," *J. Am. Ceram. Soc.*, **74** [10] 2338-92 (1991).
7. J. Liu, W. Y. Shih, R. Kikuchi, and I. A. Aksay, "Clustering of Binary Colloidal Systems: Theory," *J. Colloid Interface Sci.*, **142** (2) 369-77 (1991).
8. M. Yasrebi, W. Y. Shih, and I. A. Aksay, "Clustering of Binary Colloidal Suspensions: Experiment," *J. Colloid Interface Sci.*, **142** (2) 357-68 (1991).
9. M. Sarikaya and J. M. Howe, "Image Resolution in Conventional Transmission Electron Microscopy," in ***Proc. 49th Ann. Meeting EMSA***, edited by G. W. Bailey (San Francisco Press, San Francisco, 1991), pp. 468-69.

1992

10. F. Dogan, J. Liu, M. Sarikaya, and I. A. Aksay, "A Study on the Formation of Hydrothermally Prepared $BaTiO_3$ Particles," in ***Proc. 50th Ann. Meeting EMSA***, edited by G. W. Bailey (San Francisco Press, San Francisco, 1992), pp. 304-05.
11. G. H. Kim, M. Sarikaya, and I. A. Aksay, "Measurement of Residual Stresses in B_4C-Al Cermets by CBED," in ***Proc. 50th Ann. Meeting EMSA***, edited by G. W. Bailey (San Francisco Press, San Francisco, 1992), pp. 154-55.
12. M. Sarikaya and I. A. Aksay, "Nacre of Abalone Shell: A Natural Multifunctional Nanolaminated Ceramic-Polymer Composite Material," Chapter 1 in ***Structure, Cellular Synthesis and Assembly of Biopolymers,*** edited by Steven T. Case (Springer-Verlag, New York, 1992), pp. 1-25.
13. M. Sarikaya and I. A. Aksay, "Synthetic and Biological Nanocomposites," in ***Proceedings of the 5th International Conference on Ultrastructure Processing***, edited by L. L. Hench and J. K. West (Wiley Interscience, New York, 1992).
14. M. Sarikaya, J. T. Staley, and I. A. Aksay, "Biomimetic Materials: An Introduction," in ***Proc. 50th Ann. Meeting EMSA***, edited by G. W. Bailey (San Francisco Press, San Francisco, 1992), pp. 1020-21.
15. M. Sarikaya and I. A. Aksay, "Imaging of Hierarchically Structured Materials," in **Hierarchically Structured Materials, MRS Symp. Proc.**, Vol. 255, edited by I. A. Aksay,

E. Baer, M. Sarikaya, and D. A. Tirrell, (Materials Research Society, Pittsburgh, Pennsylvania, 1992), pp. 293-307.
16. M. Sarikaya and I. A. Aksay, "An Introduction to Biomimetics: A Structural Viewpoint," *J. Mater. Sci. and Engrn*, 1992.
17. Y. Sakka, D. D. Bidinger, J. Liu, M. Sarikaya, and I. A. Aksay, "Processing of SiC-Mullite-Al_2O_3 Nanocomposites," ***Proc. 16th Annual Conf. on Composites, Materials, and Structures*** (1992).
18. J. E. Webb and I. A. Aksay, "Low Temperature Densification of Mullite Through Transient Viscous Phase Sintering,".
19. M. Yasrebi and I. A. Aksay, "Effect of Free Polyelectrolytes on Stabilized Aqueous Suspensions,".

1993, to be submitted

20. D.-J. Rhee, G. C. Stangle, and I. A. Aksay, "The Influence of Microstructure, Degradation, and Internal Stress on Binder Removal," submitted for publication in *J. Am. Ceram. Soc.* (1991).

6. Biographical Sketches

Ilhan A. Aksay

Dr. Aksay is now a Professor in the Chemical Engineering Department and has joined the Princeton Materials Institute. Prior to joining Princeton University, Dr. Aksay was a professor in the Department of Materials Science and Engineering at the University of Washington from 1983 through August 1992. He earned his B.Sc. degree (with honors) in Ceramic Engineering at the University of Washington in 1967. He received his M.Sc. degree in 1969 and Ph.D. in 1973, both in Materials Science and Engineering at the University of California, Berkeley. Upon completing a one-year postdoctoral appointment at the University of California, Berkeley, he worked at Xerox, Webster Research Center (1973-75) and the Middle East Technical University in Ankara (1975-81). In 1981, Dr. Aksay joined UCLA's Materials Science and Engineering Department as a visiting Associate Professor. In September 1983, he joined the faculty of the University of Washington as an Associate Professor in the Department of Materials Science and Engineering and was promoted to Professor in 1985. His most recent research activities have been on the utilization of colloidal and biomimetic techniques in ceramic processing. In recognition of his contributions in this area, he received the Richard M. Fulrath Award of the American Ceramic Society in 1987. In 1987, he was also named as the first Pacific Northwest Laboratory Professor by the U.S. Department of Energy. More recently, he received the Puget Sound Engineering Council's 1988 Academic Engineer of the Year award for his "contributions to advances in ceramic processing technology and the transfer of this technology to industry and students." Dr. Aksay is a Fellow of the American Ceramic Society.

Research Interests

- processing science of ceramics
- thermodynamics and phase equilibria
- diffusion and structural studies in ionic systems
- interfacial reactions and capillary phenomena
- utilization of colloidal and biomimetic techniques in ceramic processing

Mehmet Sarikaya

Mehmet Sarikaya received his B.Sc. degree in Metallurgical Engineering from the Middle East Technical University (Ankara, Turkey) in 1977. He came to the United States on a NATO Science Scholarship for graduate studies, receiving his M.Sc. and Ph.D. degrees in Materials Science and Engineering from the University of California, Berkeley, in 1979 and 1982, respectively. In 1981, he spent the summer at the Max Planck Institut für Metallforschung, Stuttgart, West Germany. After his doctoral studies were completed, Dr. Sarikaya became a Postdoctoral Scientist at the Lawrence Berkeley Laboratory. He joined the faculty in the Department of Materials Science and Engineering as an Assistant Professor in 1986 and will be promoted to Associate Professorship in 1990. Dr. Sarikaya's research interests include high spatial resolution transmission electron microscopy (TEM); imaging, diffraction, and spectroscopy; microstructural effects upon properties in ceramics, metals, and related composites; phase transformations in ceramic and metallic systems; interface characterization; and biocrystallization. He has been the leader in expanding the microscopy facilities at the University of Washington and is currently on sabbatical at Princeton University.

Research Interests

- characterization and development of ceramic-metal composites, high-temperature ceramics, superconducting oxides, and biocomposites
- aggregation, packing, and *in situ* densification behavior of nanosized particles
- biocrystallizaton and biomimicking
- application and development of high-resolution electron microscopy techniques (imaging, diffraction, and spectroscopy)

Daniel M. Dabbs

Daniel M. Dabbs received his B.Sc. degree in Chemistry at Texas Tech University in 1977. Both his M.Sc. degree (Physical Chemistry, 1979) and Ph.D. (Materials Science and Engineering, 1984) were awarded by the University of Washington. Upon completion of his doctoral work, he went to work for Wacker Siltronic (Portland, Oregon) as a Materials Characterization Engineer. In March of 1986, Dr. Dabbs joined the research group of Dr. Ilhan A. Aksay at the University of Washington as a Postdoctoral Research Associate. A year later, he accepted the position of Acting Program Manager, Advanced Ceramics Materials Laboratory, within the Washington Technology Center and College of Engineering, University of Washington; he was promoted to Program Manager in August 1987. In September 1992 Dr. Dabbs joined Princeton University as a Research Staff Member in the Ceramic Materials Laboratory. His research interests include vibrational spectroscopic characterization of ceramics and precursors, phase transitions in ceramic precursors, fiber-matrix interaction studies, and electron transfer mechanisms. He has also performed several studies in the physical chemistry of trace elements in crystalline material. As a graduate Research Assistant, his studies on the behavior of arsenic in fayalitic slags earned him a Fellowship in the Washington Minerals Resource and Research Institute.

Research Interests

- vibrational spectroscopic characterization of ceramics and precursors
- phase transitions in ceramic precursors
- fiber-matrix interaction studies
- electron transfer mechanisms
- physical chemistry of trace elements in crystalline material